Nanopore-Based Single-Molecule Mass Spectrometry on a Lipid Membrane Microarray

Gerhard Baaken,[†,‡] Norbert Ankri,[§] Anne-Katrin Schuler,[‡] Jürgen Rühe,[‡,⊥] and Jan C. Behrends[†,⊥,*]

[†]Laboratory for Electrophysiology and Biotechnology, Department of Physiology, University of Freiburg, Hermann-Herder-Strasse 7, 79104 Freiburg, Germany, [‡]Laboratory for Chemistry and Physics of Interfaces, Department of Microsystems Engineering (IMTEK), University of Freiburg, Georges-Köhler-Allee 103, 79110 Freiburg, Germany, [§]IFR Jean Roche, Secteur Nord de la Faculté de Médecine de Marseille, Marseille 13916, France, and [⊥]Freiburg Materials Research Centre (FMF), University of Freiburg, Stefan-Meier-Strasse 21, 79104 Freiburg, Germany

ABSTRACT We report on parallel high-resolution electrical single-molecule analysis on a chip-based nanopore microarray. Lipid bilayers of <20 μm diameter containing single alpha-hemolysin pores were formed on arrays of subpicoliter cavities containing individual microelectrodes (microelectrode cavity array, MECA), and ion conductance-based single molecule mass spectrometry was performed on mixtures of poly(ethylene glycol) molecules of different length. We thereby demonstrate the function of the MECA device as a chip-based platform for array-format nanopore recordings with a resolution at least equal to that of established single microbilayer supports. We conclude that devices based on MECAs may enable more widespread analytical use of nanopores by providing the high throughput and ease of operation of a high-density array format while maintaining or exceeding the precision of state-of-the-art microbilayer recordings.

KEYWORDS: nanopore · array · polymer · mass spectrometry · alpha-hemolysin · poly(ethylene glycol) · lipid bilayer · microsystem

Biological nanopores such as the protein alpha-Hemolysin (αHL) have become promising tools for label-free single-molecule analysis. Well-known examples include detection and characterization of polynucleotides or proteins as well as synthetic polyelectrolytes,[1] single-molecule force spectroscopy, and single-molecule mass spectrometry (reviewed in refs 2, 3). Such experiments are based on potentiostatic (voltage-clamp) recordings of the pore-mediated ionic current that is modulated through partial block by single analyte molecules entering and transiently obstructing the narrow conductive path.[4,5] Protein nanopores are particularly well suited for this purpose because of their low intrinsic electrical noise, their natural ability to interact with analytes, and the possibility to modify this property in a very controlled manner (*e.g.*, by introducing specific binding sites) through molecular genetic engineering.[6] In order to work as sensors, protein nanopores have to be reconstituted in lipid bilayers separating two compartments containing aqueous electrolyte solution. For conductance (*i.e.*, voltage-clamp) recordings, these compartments must be contacted electrically by nonpolarizable electrodes. Currently, research using biological nanopores is performed using bilayers produced one at a time mostly on apertures either fabricated in hydrophobic (*e.g.*, Teflon) films[7] or at the end of a Teflon tube.[8] These platforms are being used experimentally by a number of specialized groups, but their wider practical application is limited because they require highly skilled operators and only allow one measurement at a time and because their operation is not amenable to straightforward automation. A more widespread use of protein nanopores with their many attractive applications in chemical and biological analytics will depend on the availability of recording methods that enable rapid collection of large amounts of data and that can be easily automated. However, particularly for analytical tasks that require low-noise and high-frequency bandwidth recordings, low-capacitance *micro*bilayers on smaller-than-standard (*e.g.*, < 100 μm) apertures are required,[8−10] which are not readily produced in a microarray format. A current challenge is, therefore, to provide a high-density microarray platform for parallel bilayer recording without compromising on the precision of state-of-the-art single microbilayer nanopore experiments.

In recent years, diverse microsystem approaches have produced higher-throughput versions of established membrane biophysical techniques, such as patch clamping.[11−13] The potential of such microstructured platforms to additionally provide even better signal-to-noise ratios than the original method due to smaller total capacitance has been noted.[9,10,14]

* Address correspondence to jan.behrends@physiologie.uni-freiburg.de.

Received for review July 15, 2011 and accepted September 20, 2011.

Published online September 20, 2011
10.1021/nn202670z

© 2011 American Chemical Society

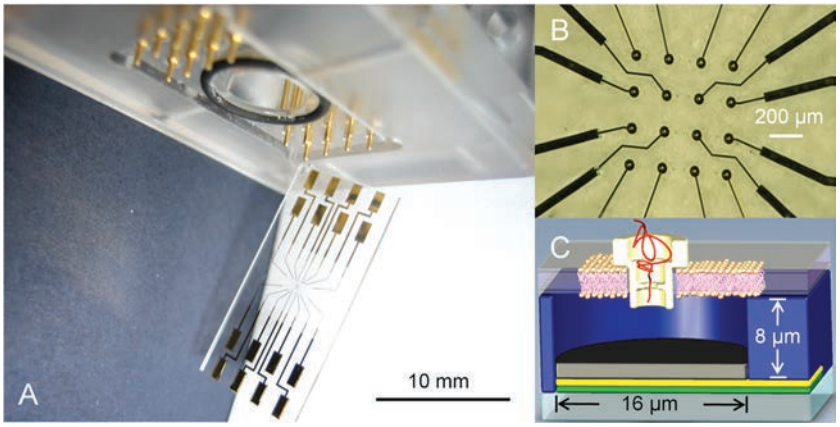

Figure 1. (A) Chip holder designed for the multielectrode cavity array (MECA) with the corresponding 16-channel MECA chip prior to insertion. The chip is inserted from below into the groove provided by the holder. The black rubber ring prevents the contact pads from being wetted by experimental fluids inserted from above into the hollow chamber (center of the holder). Spring contact pins connect the rectangular contact pads to macroscopic plugs connected to the recording electronics. (B) Magnified view of the center of the MECA microchip: Conductive pathways originating at the contact pads terminate as small circular pads arranged in a 4 × 4 array (Ø 50 μm). The whole surface is covered by an insulating polymer coating (SU8-3010). The microstructured aperture (MEC) is located on the center of each terminal pad and is considerably smaller. (C) Schematic (not to scale) view of a single MEC: The different materials are color coded: glass (light gray), Cr (green), Au (yellow), Ag/AgCl (dark gray), and SU8 (blue). By way of illustration of the experiment, an αHL nanopore in a bilayer is also shown interacting with a polymer molecule. Note, that in these experiments analytes were added from the same side as the αHL protein and will therefore enter the pore from the side of the αHL cap domain.

A number of reports have also shown recordings of currents mediated by ion channels and biological pores reconstituted in parallel bilayer arrays.[15−26] However, signal-to-noise performance and usable bandwidth in these reports have not been equivalent to the state-of-the-art in single-microbilayer experiments (*e.g.*, 200 fA rms at DC-5 kHz bandwidth).[8] This is due to the high total capacitance inherent in designs where the bilayer itself is larger than about 100 μm in diameter and/or electrical contact to both sides of the lipid bilayer is provided by macroscopic electrodes in accordingly large electrolyte volumes bounded by large surface areas. The same design properties also limit the density of integration of multiple recording sites on one substrate.

We recently reported on a microbilayer recording device based on so-called microelectrode cavities (MECs) in a dielectric polymer layer on a glass support.[27] Here, rather than on an aperture in a septum between two macroscopic compartments, artificial lipid membranes are formed over microcavities of sub-picoliter volume formed in the polymer layer, each containing an individual Ag/AgCl microdisk as the active electrode. Due to their low total capacitance (<1 pF), recordings from MEC-supported bilayers more than equal the performance of state-of-the-art microbilayers in terms of noise (*i.e.*, 125 fA rms at DC-5 kHz bandwidth under optimal screening conditions). Because of their small dimensions (diameter 6−50 μm), MECs are in principle well suited not only for high resolution but also for highly parallelized recordings from large numbers of bilayers. In the prior publication,[27] we showed simultaneous recording from two neighboring MECs in a four-channel prototype without any further validation of the device for parallel recordings. The present study now aims at ascertaining its usefulness in performing a high-resolution nanopore-based analytical task using simultaneous multichannel recordings from an array of microbilayers.

Specifically, using a 4 × 4 MEC array (MECA) we address the question whether a device based on an array of patterned Ag/AgCl-microelectrode cavities is capable of simultaneous recordings with the precision and the quantitative consistency across individual measurement sites required for an enhanced-throughput version of state-of-the-art nanopore-based single-molecule detection. We therefore decided to attempt, on a 16-channel MECA prototype, a paradigmatic experiment in nanopore analytics, nanopore-based single-molecule polymer mass spectroscopy.[28]

RESULTS AND DISCUSSION

Figure 1A shows an image of the microchip containing a MEC array with 16 elements as well as the holder designed for this particular chip layout. The 16 MECs are arranged in a 4 × 4 pattern with a regular 200 μm spacing. The active central area of the MECA chip, of which Figure 1B provides a close-up view, is, therefore, smaller than 1 mm^2. The individual connector lines entering on the periphery of the image are led to the disk-shaped electrodes. The conducting lines as well as a major part of the gold terminal pads below the MECs are covered by an 8 μm thick insulating polymer coating (SU8-3010, Microchem, Newton, MA, USA). SU8 provides a nonpolar surface (water contact angle ~85°) that is well suited for the generation of a lipid bilayer with the classical painting method. SU8 also has low relative static permittivity ($\varepsilon_r \approx 3.2$) and is inert to most

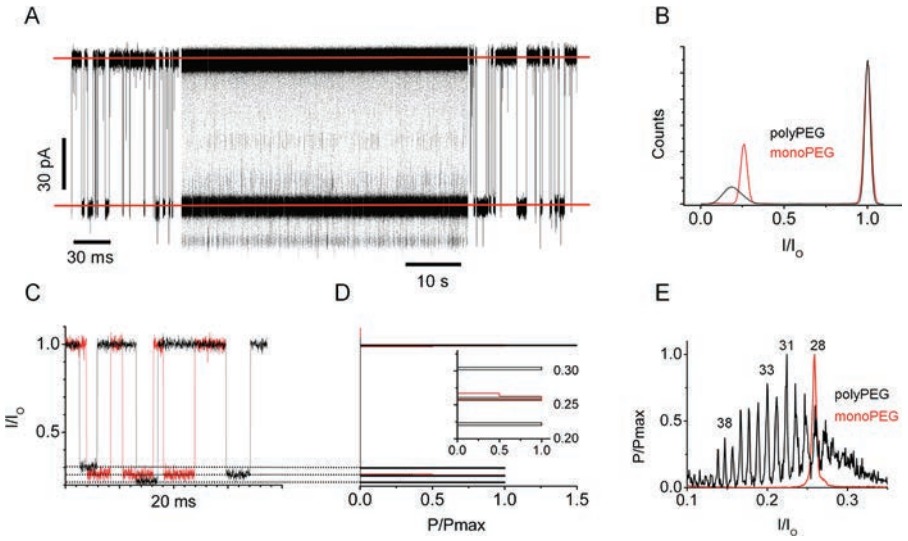

Figure 2. Current traces and histograms derived from recordings of αHL pores blocked by monoPEG-28 and polyPEG-1500 on one MEC (Φ 16 μm) of a 16-cavity chip with a SCA (Axopatch 200B) filtered at 20 kHz and digitized at 200 kHz. The MEC was held at V_h = +40 mV with respect to the *cis*-side; 4 M KCl. (A) 60 s trace of one αHL pore blocked by monoPEG. The initial and last 100 ms are shown on an expanded time scale. Note the stability of the current detected with one MEC over time (see reference lines). (B) All-points histogram of the trace shown in (A). Different distributions are obtained for monoPEG-28 (red) and polyPEG-1500 (black). Both distributions appear unimodal. (C) Three blockage events from experiments with monoPEG (red) and polyPEG (black). Note that polyPEG-induced blocks visit distinct levels. (D) Event-averaged histogram of the traces shown in (C). Probability *P* is normalized to the highest peak. Distinct levels can be clearly distinguished (polyPEG at I/I_O = 0.22, 0.26, and 0.30; monoPEG at I/I_O = 0.26). (E) Event-averaged histograms for 6.408 (polyPEG, black) or 19.318 (monoPEG, red) events (open state not shown). The multimodal distribution of polyPEG can be clearly distinguished from the monoPEG distribution. The different peaks can be assigned to the length of the particular PEG molecules of the polyPEG solution. Blockages of molecules with higher molecular weight result in lower ratios of I/I_O. With reference to the peak of the monoPEG-28-histogram (red) the peaks in the polyPEG distribution can be assigned a specific polymer size by increments or decrements of one repeat unit.[28]

common solvents as well as to many acids and bases.[29] In the center of each of the terminal pads a circular structure representing a single MEC can be discerned, the diameter of which can be controlled between 6 and 50 μm using photolithographic structuring of the SU8. At the bottom of each of these cavities a silver/silver chloride layer is deposited on the underlying Cr/Au layer, as described previously,[27] in order to provide the nonpolarizable electrode necessary for potentiostatic current (voltage-clamp) measurements. A minimum distance of 50 μm between all electronically conducting elements is preserved to avoid crosstalk (capacitive coupling) between adjacent recording channels.[27]

Electrolyte solution is added through a window in the holder opening onto the center of the microchip. The electrolyte volume required for recordings is on the order of 50 μL and forms a well-defined drop due to the wetting behavior of the nonpolar surface. This drop is contacted by an Ag/AgCl wire serving as the bath reference electrode.

To benchmark our device against state-of-the-art bilayer systems, we set out to reproduce a classic experiment by Robertson *et al.* (2007),[28] who generated a highly resolved mass spectrum of a polydisperse poley(ethylene glycol) (PEG) mixture based on measurements of the differential block of the αHL pore by individual PEG oligomers of varying sizes. The resolution that was achieved in this seminal experiment—down to single ethylene glycol repeat units (r.u.)—requires reliable and stable discrimination of current levels based on absolute differences in amplitude on the order of 1 pA. Single-molecule nanopore-based spectrometry is, therefore, well suited as a test case for a microbilayer array in a high-resolution analytical task.

As a first step, we performed this experiment recording from one of the 16 MECs on the chip using a single channel amplifier. After painting a lipid bilayer in 4 M KCl, αHL was applied to the drop of electrolyte on the chip surface (here termed *cis*-side). The Ag/AgCl electrode in the MEC was used to apply a holding potential (V_h) of +40 mV relative to the *cis*-side electrolyte drop, containing the reference electrode, so that current through any membrane conductance is driven outward. Subsequent to an insertion of a single pore, observed by a sudden drop in membrane resistivity from 20 to 30 GΩ to approximately 300 MΩ, solutions of either polydisperse (polyPEG-1500) or monodisperse PEG (monoPEG-28) were also applied to the *cis*-side of the membrane. Figure 2A shows a current trace of αHL pore blocking and unblocking transitions induced by monoPEG-28 during a period of 60 s. After Bessel filtering at a cutoff frequency of 20 kHz and digitization at a frequency of 200 kHz, the rms noise of the open pore current was 2.2 pA. Figure 2B shows histograms of the current values (*I*) of all points in the

trace normalized to the mean open pore current (I_O) for both the monoPEG-28 and the polyPEG-1500 experiment. In both cases, the open state is represented by a single Gaussian peak. Multiple open states of the αHL pore such as recently reported[30] were not observed in our experiments. The peak corresponding to the polyPEG blocked states also shows a normal-like distribution centered around $I/I_O = 0.18$, while that corresponding to monoPEG-28-blocked states shows an equally Gaussian distribution centered at $I/I_O = 0.26$. While the distribution of point values in the monoPEG-blocked states is not visibly broadened with respect to the open-state distribution, that of the polyPEG blockages is clearly much broader without, however, showing discernible peaks. Nevertheless, after digital filtering of the original trace at 5 or 1 kHz, peaks corresponding to blocks by PEG molecules of different sizes do become discernible already in the all-points histograms (not shown).

In Figure 2C, two sequences of three single blocking events, one in the presence of monoPEG-28 and the other in the presence of polyPEG, are shown superimposed. In Figure 2D, a histogram of the mean currents of the indivdual blocked states (event-averaged histogram, see Supporting Information, Supplementary Methods) constructed from the polyPEG sequence shows three discrete conductance levels, the last of which overlaps with the single level at $I/I_O = 0.26$ found for the mono-PEG-28 sequence.

Finally, in the event-averaged histogram for 6408 events detected in the 60 s recording, at least 14 peaks can be clearly detected (Figure 2E). Using the same analysis for monoPEG-28 (19 318 events collected during 1 min, red line) we find a dominant peak at a relative residual current of 0.26 exactly overlapping with one of the peaks in the polyPEG distribution, which is in full agreement with the findings of Robertson *et al*. (ref 28). We can, therefore, already from this short recording, clearly assign the peaks to the PEG oligomers from 39 to 26 r.u. The absolute mean open pore current in this experiment was 134 pA; therefore the absolute current difference per r.u. ranged from approximately 1.2 pA (39 r.u./38 r.u.) to 1.6 pA (28 r.u./27 r.u.). Peaks with smaller probabilities (>39 and <26 r.u.) are not clearly apparent due to the relatively low number ($<10^4$) of events analyzed. Furthermore, as expected,[4,28,31,32] we find a correlation between depth of block and the time constant of the monoexponential residence time distribution for each of the peaks (Supporting Information, Supplementary Data, Figure S6).

While the above experiment has shown that MECs as such support bilayer recordings of sufficiently high resolution for single-molecule nanopore-based mass spectroscopy, the specific aim of this study was to demonstrate parallel analysis by simultaneous recordings from multiple nanopores on an array. In particular, we wished to perform a parallel mass spectrometry experiment on an array of bilayers containing single nanopores to ascertain whether the results simultaneously obtained from the different recording positions quantitatively match with the necessary high precision. For these multichannel experiments, a 16-channel version of a commercially available multichannel patch-clamp amplifier (MCA, Jet-16, Tecella Inc., San Diego, CA, USA) was used instead of the single-channel patch clamp amplifier (SCA, Axopatch200B, Molecular Devices, Sunnyvale, CA, USA) used before.

An overview of the activity obtained on a 16-fold MECA in an experiment using monoPEG-28 is shown in Figure 3. Approximately 20 min after application of αHL, pore insertions and PEG-induced fluctuations were observed on a total of nine MECs. An event-averaged histogram (see Supporting Information) of the monoPEG-28-induced current transitions along with a sample trace is shown for each MEC. On seven of the MECs (01, 02, 05, 07, 08, 09, 15) current transitions mediated by the block and unblock of a single pore were observed. The corresponding conductance levels are denoted 1P1O (one pore inserted and open), 1P1B (one pore inserted and blocked), and NP (no pore insertion), respectively. By definition, the current ratio I/I_O for 1P1O is 1, whereas the residual current at 1P1B was found at $I/I_O = 0.28$. On two MECs the insertion of two pores was indicated by an additional decrease of the resistivity to 165 MΩ. Accordingly, the resulting event-averaged histogram shows three additional distinct conductance states denoted as 2P2O (two pores inserted, two open), 2P1B (two pores open, one blocked), and 2P2B (two pores inserted, both blocked). As expected, 2P2O appears at an I/I_O value of 2. 2P1B is located at a ratio of 1.28, which is exactly the sum of the values for one blocked channel and an open one. The rather improbable event of 2P2B is barely identifiable in the graphs for MEC 04 and MEC 11 but was found at a current ratio of 0.56, as expected for the sum of the residual conductances of two blocked pores. Importantly, from the dashed lines marking the different current levels, it is evident that current levels match closely between MECs.

While consistent across MECs, the residual current ratio I/I_O of 0.28 for 1P1B determined from the event-averaged histograms is clearly larger than the expected value of 0.26 (Figure 2 and ref 28). We found that this discrepancy is due to a slow frequency response (time constant of approximately 300 μs) of the Tecella Jet-16 multichannel patch clamp amplifier (MCA) employed here as opposed to the Axopatch 200B single-channel amplifier (SCA) used for our single-channel recordings (Figure 2) as well as by Robertson *et al*.[28] (see Supplementary Methods in Supporting Information, Figure S3). With such slow reponses, determining the levels of blocked states in the same way as for the single MEC experiments, *i.e*., by

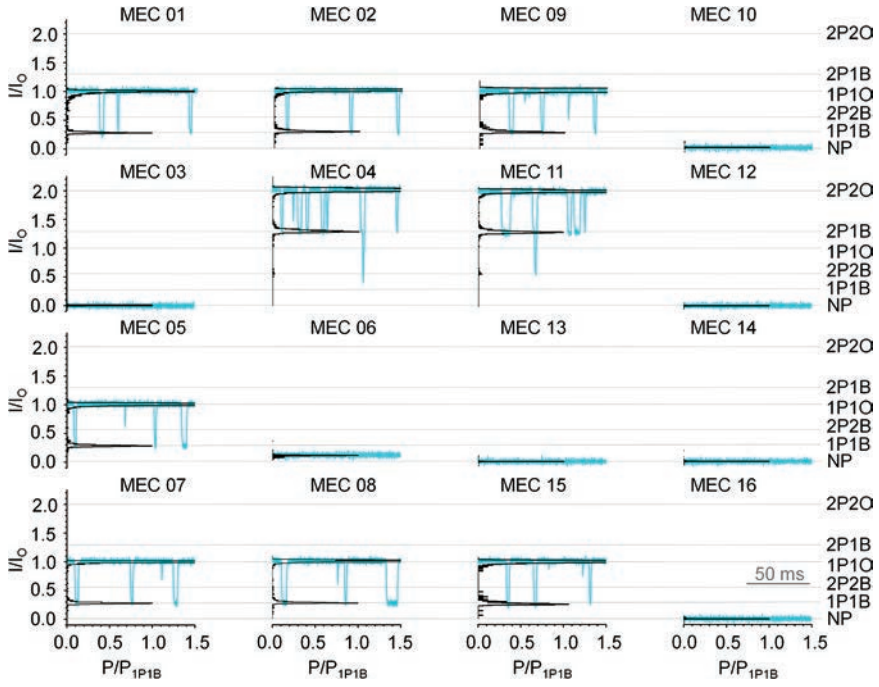

Figure 3. Event-averaged histograms (black) and overlaid current traces (cyan) of parallel and simultaneous recordings of monoPEG-28-mediated blockages of hemolysin nanopore(s) (MCA, Tecella Jet 16). In each histogram the fractional current is plotted *vs* the probability normalized to the probability of the 1P1B level (for the denotation of the conductance levels see text). Histograms were derived from the mean current levels of at least 2000 visits of blocked states per cavity (20 kHz sampling frequency). Current traces are shown isochronously for a period of 100 ms ($V_h = +40$ mV). The absence of crosstalk between neighboring recording sites and the agreement of levels across MECs can be appreciated.

averaging all data points beyond a threshold value, however, leads to I/I_O values that are too high. Using an alternative measurement of current levels based on a fit to the exponential time course of the MCA's response to step changes in conductance, we arrived at the expected value of 0.26 (see Supplementary Methods in Supporting Information, Figure S5).

An interesting feature of parallel multichannel bilayer arrays is the direct representation they offer of both the probabilistic nature of the membrane insertion process and the variety of protein nanopores in an αHL preparation. We have not studied this systematically, as we varied experimental conditions (lipid concentration, applied voltage,[33] αHL concentration) according to the progress of each experiment. In a database of 15 experiments with 16-fold MECAs (*i.e.*, 240 bilayers), we thus obtained 70 insertions of one solitary, well-oriented, *bona fide* αHL pore. The number of such successful single-pore insertions per 16-channel MECA varied between a minimum of 0 and a maximum of 9 and averaged 4.7. The remaining MECs had no insertion ($n = 121$, min./MECA = 1, max./MECA = 15, av/MECA = 8.1), insertion of more than one pore ($n = 9$, min./MECA = 0, max./MECA = 3, av/MECA = 0.6), or insertion of pores with lower (50−75% of αHL) conductance ($n = 29$, min./MECA = 1, max./MECA = 11, av/MECA = 0.6), the latter likely representing impurities in the αHL preparation we used. A further minority of insertions ($n = 11$, min./MECA = 0, max./MECA = 3, av/MECA = 0.7) were pores having αHL-like conductance but displaying only very short-lived PEG-mediated blocking events with the MEC held at positive potentials, while reversing the polarity of the applied field yielded blocking events of the expected duration. Indeed, it has been shown that the residence time of PEG molecules inside the αHL pore shows nonlinear and asymmetric voltage dependence.[31] In the presence of 1−4 M KCl, the longest residence times were measured when the transmembrane potential difference was near +40 mV, with the positive potential oriented away from the pore's head domain, while an oppositely oriented but equally large potential difference resulted in an up to 10-fold reduction in residence times.[31] We thus conclude that the short-lived events were recorded from maloriented αHL pores due to re-formation of bilayers after rupture (see also Supporting Information, Supplementary Data, Figure S7).

An advantage of array-format parallel recording systems is to improve information yield by increasing the sample size and to reduce the time required to arrive at a statistically robust result. Alternatively, array formats can be used to simultaneously analyze multiple samples. In each case, it is important that the quantitative match between results from each recording site is as precise as possible. While the frequency response of the patch clamp MCA predictably limits the resolution of the analysis, especially for the shorter

polymers, we nevertheless went on to simultaneously record polyPEG-1500 on the 16-channel MECA to produce mass spectra from multiple simultaneous recordings and determine their consistency. For the histograms displayed in Figure 4A–G, simultaneous single-pore recordings were obtained during 60 s at a holding potential (V_h) of +60 mV in 3 M KCl. Traces from seven out of 16 MECs delivered stable, single-pore data (see Supporting Information, Supplementary Data Figure S7) and were analyzed using monoexponential fit-based measurement of current levels (see Supporting Information). For all histograms, peaks in the range $0.13 < I/I_O < 0.23$ are clearly resolved. Importantly, the position of the maxima agrees well between MECs (broken lines in Figure 4). For current ratios of less than 0.13 and of more than 0.23 the histograms of the single MECs clearly show differences in the degree of resolution of the single peaks. Again, this is primarily a consequence of the—deliberately chosen—short recording times and therefore the relatively low number of events detected. Additionally, the time constants of the single channels of the MCA varied by about 60 μs from 260 μs for the fastest to 320 μs for the slowest. Therefore, the sharpness of peaks in the histograms is also affected by the choice of the time constant of the exponential fit used for event analysis (for details see Supporting Information, Supplementary Methods). However, in the histogram of all detected events combined from all MECs (H) the single peaks—even at the low and high extremes of I/I_O—are clearly visible and correspond precisely to the peaks in the single-MEC histograms, A–G. Overall, 17 peaks can be observed reflecting αHL block by polymer chains with repeat units from 28 (overlapping with the distribution from the monoPEG-28 recording, red columns) to 44. For these experiments, the potential of the MEC was held at +60 mV relative to the *cis*-side (instead of +40 mV, as in the experiment shown in Figure 2). This was done to enhance the frequency of blocks[31] and thereby enhance the resolution of peaks caused by the partitioning into the pore of longer polymers. Simultaneously, this resulted in a shift of all peaks toward higher current ratios compared to the single-channel results (Figure 2), with the peak for monoPEG-28 at an I/I_O ratio of 0.275 (see also ref 32).

Our single-channel results (Figure 2) clearly show that limited time resolution, and the resulting need for fitting of time constants in order to determine current levels, is not a a property of the MECA device, but of the multichannel amplifier, and can be remedied in future devices. The availability for nanopore analytics of high-resolution bilayer array platforms based on the MECA or on further versions of other designs[15–26] is likely to strengthen efforts to develop multichannel voltage-clamp amplifiers (*e.g.*, ref 23) that are more precisely adapted to the needs of bilayer recording and hopefully less expensive than those currently available.

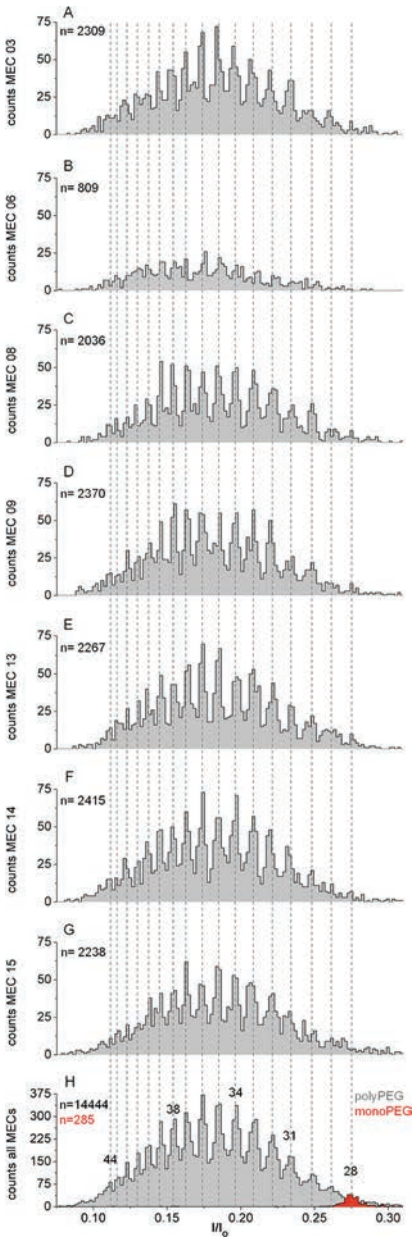

Figure 4. Histograms of normalized residual currents levels during PEG-induced blockages of single αHL pores recorded with the MCA (60 s recording time). The current levels were measured by exponential fitting (see text and Supporting Information, Supplementary Methods, for details). Events with durations shorter than 2.5 ms were excluded. (A–G) Individual event-averaged histograms derived from seven simultaneously acquired single-pore recordings from a MECA (one histogram per MEC). For primary traces see Supporting Information, Supplementary Data, Figure S7. Broken vertical lines indicate the agreement of the position of maxima between MECs. (H) Histogram of the combined events detected on all seven MECs during this experiment. A histogram of events derived from the recording of monoPEG-28-induced blocks of a single αHL pore (red columns) is superimposed to define the current ratio for 28 repeat units at I/I_O = 0.275 by way of calibration. The shift in the position of maxima with respect to the data in Figure 2 is due to a higher driving force (V_h = +60 mV, 3 M KCl, for details see text).

It has been supposed that a possible specific limitation of the MECA design could be a lack of long-term

stability of Ag/AgCl microelectrodes due to a finite reservoir of redox electrode materials.[34] During our electroplating procedure, we apply 10 nA of current to each MEC for between 4.5 and 10 min, corresponding to a charge deposited in the form of Ag of between 2.7 and 6 μC. Operating the device at a positive holding potential, we can therefore expect to deliver, for example, 150 pA for between 5 and 11 h before all Ag is converted into AgCl. However, the buildup of low-conductivity AgCl may pose a problem for long-term stable measurements. In fact, we did sometimes observe increases in MEC series resistance in early experiments, where MECs were repeatedly used without restoring the electrode material. However, as shown in the Supporting Information, Supplementary Data, Figure S8, freshly silver-plated and partially chloridized MECs can support nanopore recordings for more than 90 min without a decrease in open pore current. In fact, such long-term recordings (n = 7) were always terminated by an instantaneous disappearance of the pore current, suggestive of irreversible closure or deinsertion of the pore rather than a gradual decline expected for an increase in series resistance or electrochemical exhaustion.

CONCLUSION

Using a polymer mass spectrometry experiment as a benchmark, we have shown high-resolution single-molecule analysis by measurements of nanopore conductance on a chip-based nanopore array. Parallel recordings with a commercially available multichannel patch-clamp amplifier allowed detection of single peaks in the distributions linked to blockage of the pore by polymers of different length. We note that compared to the single-channel recording on the same platform, the resolution of the parallel assay was somewhat limited by the slow time constant of the multichannel patch-clamp amplifier used. As shown by the single MEC measurements on the same MECA but using a state-of-the-art single-channel amplifier, the MECA device is not inherently limiting as far as signal-to-noise ratio is concerned. Due to the low capacitance of the MECs, the rms open pore current noise in our experiments using the SCA (see Figure 2) was 2.2 pA at a bandwidth of 20 kHz (0.9 pA following digital filtering at 10 kHz).

Recently, Reiner *et al.*[32] have shown nanopore-based mass spectrometry experiments using bilayers formed on small-aperture quartz pipets and a custom-built amplifier with exceptionally low input capacitance (<300 fF), which has enabled them to extend the recording bandwidth to 100 kHz. It would, therefore, appear that a multichannel version of an amplifier with such properties would be ideally suited for use with the MECA chip device to enable the whole range of single-molecule nanopore experiments to be performed with greater ease and throughput as well as a resolution improved over established techniques.

MECA chips can be produced in cost-efficient batch processes and rapidly tailored to different formats according to the needs of the experimenter. Formats allowing for simultaneous recording of data from multiple pores under identical experimental conditions will greatly reduce recording times, while the ability to simultaneously record from multiple pores in the presence of different analytes may also be attractive. Due to its hydrophobic surface, bilayer formation on the MECA is no more difficult than on a classical single aperture device, but the configuration may also be adapted for automation of this crucial step, *e.g.*, by integration of *cis*-side microfluidic channels or by mechanical automation of painting procedures. Finally, the open configuration of the upper (*cis*) side allows the use of dispensing and pipetting robots for wholly unattended operation.

METHODS

Manufacture of Microelectrode-Cavity Arrays. After spin coating a sacrificial layer of photoresist (AZ 5214E, MicroChemicals, Ulm, Germany) on a Pyrex wafer substrate and exposing the resist through a photolithographical mask (Deltamask, Enschede, The Netherlands) at 365 nm, two metal layers (Cr 20 nm, Au 200 nm) were successively deposited by electron evaporation. The sacrificial layer was removed in a lift-off process (AZ developer, MicroChemicals, Ulm, Germany), and a layer of SU8-3010 (Microchem, Newton, MA, USA) was spun on the surface and structured with a second photolithographical mask (Deltamask, Enschede, The Netherlands) and developed (SU8 developer, Microchem, Newton, MA, USA). Afterward the wafer was diced, and each of the MECs was electroplated with silver (0.5 M $NH_{3(aq)}$, 1 mM $AgNO_3$) applying 10 nA for 4.5 min (16 μm MECs) and 14.0 min (20 μm MECs), respectively, with a multichannel amplifier (Jet-16, Tecella, Costa Mesa, CA, USA). Within a final step the Ag layers were partially chloridized in 3 M KCl with 10 nA for 2.25 min (16 μm MECs) and 7 min (20 μm MECs), respectively.

Lipid Bilayer Formation and Recording. Lipid solutions were prepared from 1,2-diphytanoyl-*sn*-glycero-3-phosphocholine (DPhPC, Avanti Polar Lipids, Alabaster, AL, USA) dissolved in octane (Sigma Aldrich, Munich, Germany) at a concentration of 2 mg/mL. A 4 M (Figures 2 and 3) or 3 M (Figure 4) KCl solution (Sigma Aldrich (Fluka), Munich, Germany), 5 mM Tris, buffered at pH 7.43 was used as electrolyte. αHL (α-hemolysin from *Staphylococcus aureus*, lyophilized powder, protein ~60%, Sigma Aldrich, Munich, Germany) was dissolved and stored in DI water at a concentration of 2.5 μg/mL. Monodisperse poly(ethylene glycol) (monoPEG-28, M_w = 1251 g/mol, "PEG-28", Polypure, Oslo, Norway) and polydisperse poly(ethylene glycol) (polyPEG-1500, M_w = 1400−1600 g/mol, "poly(ethylene glycol) FLUKA", Sigma Aldrich, Munich, Germany) were dissolved in the electrolyte solution to a concentration of 10 mg/mL. For bilayer formation, the chamber of the holder was filled with 40 μL of electrolyte solution. A lipid bilayer was painted on the chip surface by briefly dipping the tip of a 20 mm (L) × 2 mm (W) × 0.5 mm (T) PTFE (VWR, Darmstadt, Germany) in the lipid solution and subsequently swiping the surface. To initiate pore insertion, 5 μL of an αHL stock solution was added to the *cis*-side solution drop, resulting in a final concentration of approximately 0.3 μg/mL. A silver wire with a diameter of 0.25 mm (VWR, Darmstadt, Germany) was chloridized in 150 mM KCl and inserted at the top

of the holder into the electrolyte serving as a bath reference electrode. After pore insertion, monoPEG-28 or polyPEG-1500 was also added *cis*-side to a final concentration of 0.4 mg/mL. Single bilayer recordings were performed with a single-channel amplifier (Axopatch 200B, Molecular Devices, Sunnyvale, CA, USA) in capacitive feedback mode. The built-in 4-pole Bessel filter was set to its maximal cutoff freuqency (f_c) of 100 kHz, and an external low-pass filter (Frequency Devices 9002, Ottawa, IL, USA) was looped in and set to a f_c = 20 kHz (8 pole Bessel). SCA data were digitized using an NI-PCI 6221 AD converter (National Instruments, Austin, TX, USA) controlled by GePulse software (Michael Pusch, Genova, Italy).

Simultaneous recordings of 16 bilayers were performed with a multichannel-patch-clamp amplifier (MCA, Jet-16, Tecella Inc., Costa Mesa, CA, USA) with a 500 MΩ feedback resistor and digitized using the integrated AD converter with a sampling rate of 20 kHz. The integrated low-pass Bessel filter was set to f_c = 3.11 kHz. In all experiments illustrated, the MEC was held at a positive potential of either +40 mV (Figures 2 and 3) or +60 mV (Figure 4) relative to the *cis*-side reference electrode, resulting in an outward current accross the membrane spanning the MEC. Current traces were exported into Axon binary format (ABF) files for event detection, further analysis, and display.

Event Detection and Data Analysis. Transitions between the open state and PEG-induced blocked states (and *vice versa*) of αHL pores were automatically detected using a modified version of the LabView (National Instruments, Austin, TX, USA) based software "Detectivent" originally developed by N.A. for detecting neuronal synaptic events and which performs a thresholding algorithm on a rectified signal derived from the original current trace. Blocked- and open-state current levels were initially determined by averaging all data points between the end of one state transition and the onset of the next (point averaging method). In order to account for the slow frequency response of the MCA, this method was substituted by monoexponential fits of the individual transitions of the form $I(t) = I_{max} - (e^{-\tau/t})$ with I_{max} as the only free parameter. For detailed information on detection of transitions and determination of current levels see Supplementary Methods in the Supporting Information (Figures S1−S5).

Further analysis and display of current traces and detection results was performed using IgorPro (Wavemetrics, Lake Oswego, OR, USA) including NeuroMatic XOPs (Jason Rothman, ThinkRandom, London, UK) or Origin (Originlab, Northampton, MA, USA) software.

Acknowledgment. The authors thank M. Vellinger, N. Lehmann, and M. Reichel for technical help. This work was funded by the Federal Ministry of Education and Research (BMBF) within the project PolyEPhys (FKZ 0315316B).

Supporting Information Available: Additional experimental details, a detailed description of the event detection algorithm, the effect of the amplifier requency response on current level measurements, as well as supplementary data regarding residence times, the original traces of the multichannel recording analyzed in Figure 4, and an example of long-term recordings on the MECA. This material is available free of charge *via* the Internet at http://pubs.acs.org.

REFERENCES AND NOTES

1. Murphy, R. J.; Muthukumar, M. Threading Synthetic Polyelectrolytes through Protein Pores. *J. Chem. Phys.* **2007**, *126*, 051101-1–4.
2. Kasianowicz, J. J.; Robertson, J. W. F.; Chan, E. R.; Reiner, J. E.; Stanford, V. M. Nanoscopic Porous Sensors. *Annu. Rev. Anal. Chem.* **2008**, *1*, 737–766.
3. Majd, S.; Yusko, E. C.; Billeh, Y. N.; Macrae, M. X.; Yang, J.; Mayer, M. Applications of Biological Pores in Nanomedicine, Sensing, and Nanoelectronics. *Curr. Opin. Biotechnol.* **2010**, *21*, 439–476.
4. Krasilnikov, O. V.; Rodrigues, C. G.; Bezrukov, S. M. Single Polymer Molecules in a Protein Nanopore in the Limit of a Strong Polymer-Pore Attraction. *Phys. Rev. Lett.* **2006**, *97*, 018301.
5. Bayley, H.; Martin, C. R. Resistive-Pulse Sensing - from Microbes to Molecules. *Chem. Rev.* **2000**, *100*, 2575–2594.
6. Maglia, G.; Heron, A. J.; Stoddart, D.; Japrung, D.; Bayley, H. Analysis of Single Nucleic Acid Molecules with Protein Nanopores. *Methods Enzymol.* **2010**, *475*, 591–623.
7. Hanke, W.; Schlue, W. R. *Planar Lipid Bilayers: Methods and Applications*; Academic Press: London, 1993.
8. Akeson, M.; Branton, D.; Kasianowicz, J. J.; Brandin, E.; Deamer, D. W. Microsecond Time-Scale Discrimination among Polycytidylic Acid, Polyadenylic Acid, and Polyuridylic Acid as Homopolymers or as Segments within Single RNA Molecules. *Biophys. J.* **1999**, *77*, 3227–3233.
9. Mayer, M.; Kriebel, J. K.; Tosteson, M. T.; Whitesides, G. M. Microfabricated Teflon Membranes for Low-Noise Recordings of Ion Channels in Planar Lipid Bilayers. *Biophys. J.* **2003**, *85*, 2684–2695.
10. Sondermann, M.; George, M.; Fertig, N.; Behrends, J. C. High-Resolution Electrophysiology on a Chip: Transient Dynamics of Alamethicin Channel Formation. *Biochim. Biophys. Acta: Biomembranes* **2006**, *1758*, 545–551.
11. Fertig, N.; Blick, R. H.; Behrends, J. C. Whole Cell Patch Clamp Recording Performed on a Planar Glass Chip. *Biophys. J.* **2002**, *82*, 3056–3062.
12. Fertig, N.; Klau, M.; George, M.; Blick, R. H.; Behrends, J. C. Activity of Single Ion Channel Proteins Detected with a Planar Microstructure. *Appl. Phys. Lett.* **2002**, *81*, 4865–4867.
13. Dunlop, J.; Bowlby, M.; Peri, R.; Vasilyev, D.; Arias, R. High-Throughput Electrophysiology: An Emerging Paradigm for Ion-Channel Screening and Physiology. *Nat. Rev. Drug Discovery* **2008**, *7*, 358–368.
14. Sigworth, F. J.; Klemic, K. G. Microchip Technology in Ion-Channel Research. *IEEE Trans. NanoBiosci.* **2005**, *4*, 121–127.
15. Peterman, M. C.; Ziebarth, J. M.; Braha, O.; Bayley, H.; Fishman, H. A.; Bloom, D. M. Ion Channels and Lipid Bilayer Membranes under High Potentials Using Microfabricated Apertures. *Biomed. Microdevices* **2002**, *4*, 231–236.
16. Sandison, M. E.; Morgan, H. Rapid Fabrication of Polymer Microfluidic Systems for the Production of Artificial Lipid Bilayers. *J. Micromech. Microeng.* **2005**, *15*, S139–S144.
17. Suzuki, H.; Tabata, K. V.; Noji, H.; Takeuchi, S. Highly Reproducible Method of Planar Lipid Bilayer Reconstitution in Polymethyl Methacrylate Microfluidic Chip. *Langmuir* **2006**, *22*, 1937–1942.
18. Sandison, M. E.; Zagnoni, M.; Abu-Hantash, M.; Morgan, H. Micromachined Glass Apertures for Artificial Lipid Bilayer Formation in a Microfluidic System. *J. Micromech. Microeng.* **2007**, *17*, S189–S196.
19. Le Pioufle, B.; Suzuki, H.; Tabata, K. V.; Noji, H.; Takeuchi, S. Lipid Bilayer Microarray for Parallel Recording of Transmembrane Ion Currents. *Anal. Chem.* **2008**, *80*, 328–332.
20. Hromada, L. P.; Nablo, B. J.; Kasianowicz, J. J.; Gaitan, M. A.; DeVoe, D. L. Single Molecule Measurements within Individual Membrane-Bound Ion Channels Using a Polymer-Based Bilayer Lipid Membrane Chip. *Lab Chip* **2008**, *8*, 602–608.
21. Zagnoni, M.; Sandison, M. E.; Morgan, H. Microfluidic Array Platform for Simultaneous Lipid Bilayer Membrane Formation. *Biosens. Bioelectron.* **2009**, *24*, 1235–1240.
22. Poulos, J. L.; Jeon, T. J.; Damoiseaux, R.; Gillespie, E. J.; Bradley, K. A.; Schmidt, J. J. Ion Channel and Toxin Measurement Using a High Throughput Lipid Membrane Platform. *Biosens. Bioelectron.* **2009**, *24*, 1806–1810.
23. Thei, F.; Rossi, M.; Bennati, M.; Crescentini, M.; Lodesani, F.; Morgan, H.; Tartagni, M. Parallel Recording of Single Ion Channels: A Heterogeneous System Approach. *IEEE Trans. Nanotechnol.* **2010**, *9*, 295–312.
24. Maurer, J. A.; White, V. E.; Dougherty, D. A.; Nadeau, J. L. Reconstitution of Ion Channels in Agarose-Supported Silicon Orifices. *Biosens. Bioelectron.* **2007**, *22*, 2577–2584.
25. Suzuki, H.; Tabata, K.; Kato-Yamada, Y.; Noji, H.; Takeuchi, S. Planar Lipid Bilayer Reconstitution with a Micro-Fluidic System. *Lab Chip* **2004**, *4*, 502–505.

26. Osaki, T.; Suzuki, H.; Le Pioufle, B.; Takeuchi, S. Multichannel Simultaneous Measurements of Single-Molecule Translocation in Alpha-Hemolysin Nanopore Array. *Anal. Chem.* **2009**, *81*, 9866–9870.
27. Baaken, G.; Sondermann, M.; Schlemmer, C.; Ruhe, J.; Behrends, J. C. Planar Microelectrode-Cavity Array for High-Resolution and Parallel Electrical Recording of Membrane Ionic Currents. *Lab Chip* **2008**, *8*, 938–944.
28. Robertson, J. W. F.; Rodrigues, C. G.; Stanford, V. M.; Rubinson, K. A.; Krasilnikov, O. V.; Kasianowicz, J. J. Single-Molecule Mass Spectrometry in Solution Using a Solitary Nanopore. *Proc. Natl. Acad. Sci. U. S. A.* **2007**, *104*, 8207–8211.
29. Chang, Y. J.; Mohseni, K.; Bright, V. M. Fabrication of Tapered Su-8 Structure and Effect of Sidewall Angle for a Variable Focus Microlens Using EWOD. *Sens. Actuators, A* **2007**, *136*, 546–553.
30. Robertson, J. W. F.; Kasianowicz, J. J.; Reiner, J. E. Changes in Ion Channel Geometry Resolved to Sub-Angstrom Precision Via Single Molecule Mass Spectrometry. *J. Phys.: Condens. Matter* **2010**, *22*, 454108.
31. Rodrigues, C. G.; Machado, D. C.; Chevtchenko, S. F.; Krasilnikov, O. V. Mechanism of KCl Enhancement in Detection of Nonionic Polymers by Nanopore Sensors. *Biophys. J.* **2008**, *95*, 5186–5192.
32. Reiner, J. E.; Kasianowicz, J. J.; Nablo, B. J.; Robertson, J. W. F. Theory for Polymer Analysis Using Nanopore-Based Single-Molecule Mass Spectrometry. *Proc. Natl. Acad. Sci. U. S. A.* **2010**, *107*, 12080–12085.
33. Renner, S.; Bessonov, A.; Simmel, F. C. Voltage-Controlled Insertion of Single A-Hemolysin and Mycobacterium Smegmatis Nanopores into Lipid Bilayer Membranes. *Appl. Phys. Lett.* **2011**, *98*, 083701.
34. Lemay, S. G. Nanopore-Based Biosensors: The Interface between Ionics and Electronics. *ACS Nano* **2009**, *3*, 775–779.